*Friction* **11**(6): 911–926 (2023)
https://doi.org/10.1007/s40544-022-0630-9
ISSN 2223-7690
CN 10-1237/TH
RESEARCH ARTICLE

# Effect of functional groups on tribological properties of lubricants and mechanism investigation

**Hongxiang YU[1,2], Haijie CHEN[1,2], Zhiwen ZHENG[1,2], Dan QIAO[1,*], Dapeng FENG[1,*], Zhenbin GONG[1], Guojun DONG[1]**

[1] *State Key Laboratory of Solid Lubrication, Lanzhou Institute of Chemical Physics, Chinese Academy of Sciences, Lanzhou 730000, China*

[2] *Center of Materials Science and Optoelectronics Engineering, University of Chinese Academy of Sciences, Beijing 100049, China*

*Received: 14 December 2021 / Revised: 18 January 2022 / Accepted: 01 April 2022*



**Abstract:** Nine organic compounds were utilized as model lubricants to investigate the impact of functional groups on tribological performances. Nonanoic Acid with carboxyl showed the best lubrication properties, and fluid film and tribofilm were coexistent in its friction test, bringing a low friction coefficient and wear rate. In addition, the lubricant with low friction coefficient corresponded to high adsorption energy in density functional theory (DFT) calculations. And the lubricant forming adsorption film with large surface energy displayed small wear rate in friction test. Moreover, adsorption energies positively correlated surface energies. Based on the experimental results, the action mechanism of functional groups on tribological properties of lubricants was proposed. Various functional groups make lubricant molecules show different adsorption energies and surface energies. Lubricant molecules with high adsorption energy are more likely to adsorb on substrates and form a vertical monolayer, which can maintain a regular molecular brush structure during friction and bring a low friction coefficient. And lubricant molecules with high surface energy may be more prone having tribochemical reactions during friction and forming protective tribofilm, which leads to a low wear rate.

**Keywords:** functional group; tribological property; adsorption energy; surface energy; action mechanism

## 1 Introduction

Energy consumption owing to friction accounts for 23%, approximately 119 EJ, of global energy consumption [1, 2]. In present industrialized nations, financial wastage brought by friction and wear is as high as about 6% of GDP [1, 3]. In order to protect the environment and reduce economic loss, frictional energy losses and wear should be minimized [4–6], which requires higher energy efficiency of mechanical system [7, 8]. Lubricants with low viscosity are beneficial to improve energy utilization through diminishing fluid friction in the hydrodynamic lubrication regime [8, 9]. However, there is insufficient lubricant on the sliding interface for the boundary and mixed lubrication where the direct contact of frictional pairs increases friction and wear [9–12]. Adding organic friction modifiers (OFMs) or anti-wear additives to low viscosity lubricants is considered to be an effective method to bring excellent lubrication effect in different lubrication regimes [10, 11, 13].

As an important class of lubricant additives, OFMs are typical amphiphilic surfactant molecules with non-polar aliphatic tail groups and polar head groups [3, 8, 10, 12, 14, 15]. The polar head groups can adsorb on the substrate surface, and long aliphatic tail groups align outward into the lubricating oil, forming close-packed self-assembled monolayers [14, 16–22]. The intermolecular van der Waals force makes the adsorption layer very strong [8]. Under the action of

* Corresponding authors: Dan QIAO, E-mail: ddqiao@licp.cas.cn; Dapeng FENG, E-mail: dpfeng@licp.cas.cn

load and shear, the incompressible adsorption layer is toilless to slip between opposite polar groups, resulting in reduction of friction and wear [12, 14]. Adsorption of OFMs is influenced by many factors, including temperature, molecular structure, and concentration. The hydrocarbon chain length could influence thickness and stacking density of the adsorption layer [16, 17]. Shi et al. [12] utilized molecular dynamics simulation to investigate the physisorption on hydroxylated $SiO_2$ (001) surfaces of OFMs dissolved in 1-decene trimer (PAO4). The results indicated that OFM molecules formed intensive and perpendicular monolayers under lower temperature. However, the adsorbed films became unconsolidated under higher temperature. Fry et al. [15] used the quartz crystal microbalance (QCM) and spectroscopic ellipsometry to measure the adsorbed layer thickness of OFMs in hexadecane. It was found that the thickness of the adsorption layer depended on the concentration and structure of OFMs. And saturated linear chains would produce the thickest film. At the same time, they studied the interactions between OFM additives and found that oleic acid and oleylamine can produce ionic liquid, bringing enhanced antifriction performance [9].

The friction reduction performance of OFMs is affected by multiple factors: dipole interaction among polar groups, dispersive interaction among hydrocarbon tails, mutual effect between adsorbate and sliding interface [8], and the kinetics of OFMs deposition and removal [23]. The tribological properties of OFMs are related tightly to their structures, including the reaction activity of polar head groups, molecular chain length, and unsaturation degrees of OFMs. Ouyang et al. [3] found that glyceryl monostearate (GMS) and glyceryl monoelaidate (GME) exhibited better tribological performances compared to glyceryl monooleate (GMO). During film formation, the GMO stretched out horizontally due to the existence of its cis double bond, resulting in more loss of conformational entropy, the lower surface coverage of tribofilm, and the worse lubricating properties. Beltzer [24] discovered that oleic acid, elaidic acid, and stearic acid performed increased lubrication property on metal substrate covered by polytetrafluoroethylene (PTFE). Kuwahara et al. [6] found that glycerol or unsaturated fatty acids between ta-C/ta-C tribopairs can bring ultra-low friction. Atomistic simulations revealed that multiple reactive centers of unsaturated fatty acids or glycerol could adsorb on ta-C surface and bridge the friction gap, and a series of molecular fragmentation reactions were induced by mechanical strain to achieve ultra-low friction.

In previous studies, these OFMs were mostly used as additives to study their properties [8, 14, 25–28]. However, the existence of base oil would have an inevitable effect on the study of tribological properties of OFMs with different structures. Therefore, in this work, pure OFMs with different functional groups were chosen as model lubricants to study the impact of functional groups on tribological properties systematically. Nine model lubricants were tested under the same frictional conditions. Afterwards wear debris was analyzed by Raman spectroscopy to determine its components, and wear scars of disks were analyzed by scanning electron microscopy and energy dispersive spectroscopy (SEM–EDS) to investigate the wear mechanisms. And the lubrication mechanism of Nonanoic Acid with excellent tribological properties was further explored by Raman spectroscopy, X-ray photoelectron spectroscopy (XPS), and transmission electron microscopy (TEM) analyses. Furthermore, the surface energies after the adsorption film formation and adsorption energies of lubricant molecules on steel surface were obtained separately by contact angle tests and density functional theory (DFT) simulations. Finally, the action mechanism of functional groups on lubrication performance of lubricants was proposed.

## 2 Materials and methods

### 2.1 Materials

The chemical reagents (Fig. 1) obtained from Aladdin Co., Ltd. (China) were applied as model lubricants to investigate the impact of different functional groups on lubrication performance of lubricants. They were n-Nonane, 1-Nonene, 2-Nonanone, Nonanal, 1-Nonanethiol, 1-Nonylamine, 1-Nonanol, Nonanoic Acid, and 4-n-Propylphenol. All lubricants were ≥ 95% in purity and were used as received. Petroleum ether, n-hexane, and diiodomethane with analytical grade were purchased from Macklin Co., Ltd. (China).

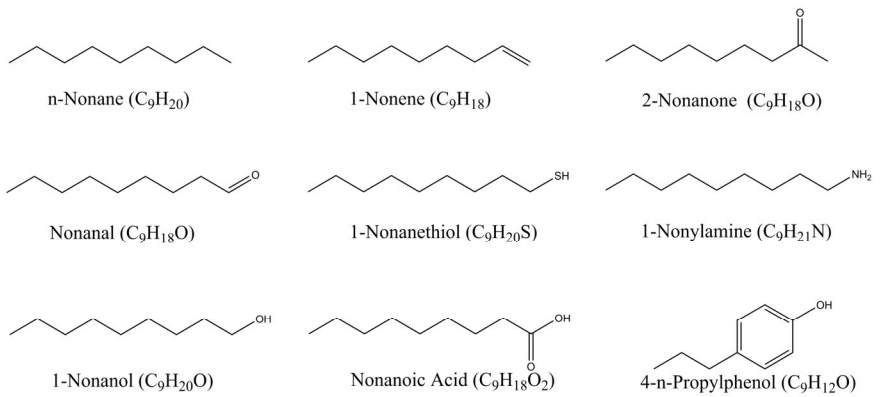


**Fig. 1** Chemical structures of model lubricant molecules employed in the study.

The friction tests were conducted with ball-on-disk friction pair (GCr15 steel). The surface roughnesses (*Sa*) of disks and balls are <10 and <30 nm, respectively. The hardness of stationary disks (GCr15, ø24.0 mm × 7.9 mm) is 750–800 HV. The diameter of upper running balls (GCr15) is 6 mm, and their hardness is 700–750 HV.

### 2.2 Tribological test

Tribological tests were carried out using a universal mechanical tester (UMT) friction testing machine, which contains a rotating disk and a stationary ball. Before the test, they underwent ultrasonic cleaning in petroleum ether for 30 min. In the tribological test, 0.05 mL lubricant was injected on the friction surface. At room temperature (RT), the frictional experiment was conducted for 60 min under a rotational speed of 90 r·min$^{-1}$ and a stationary force of 10 N. The maximum Hertz contact stress was 1.6 GPa with sliding speed of 18.8 mm·s$^{-1}$. To ensure the accuracy of the data, each test was conducted three times.

### 2.3 Characterizations

Prior to frictional experiments, the chemical structures of model lubricants were confirmed with the help of Fourier transform infrared (FTIR) spectrometer (Nicolet iS10, Thermo Fisher Scientific). After tribological test, the Raman microscope (LabRAM HR Evolution, Horiba) was applied to characterize wear scar and debris (ND filter = 10%, laser = 532 nm). Afterwards wear scars of disks were wiped by absorbent cottons soaked in petroleum ether for cleaning the friction surface. The morphology and wear volume of wear scars were acquired with the assistance of the scanning electron microscope (JSM-5601LV, FEI) and 3D profiler (MicroXAM, KLA-Tencor). The elemental compositions and chemical states of sliding surfaces were inspected by the X-ray photoelectron spectrometer (PHI5000, Thermo Fisher Scientific) with the exciting source of Al K$\alpha$ radiation. The elastic modulus and hardness of blank steel and wear scar were studied by the nano-indenter. The transmission electron microscope (TEM; JEM-F200, JEOL) was applied to acquire micrographs of wear debris.

### 2.4 Calculation of adsorption energy

All DFT calculations were conducted using the Perdew–Burke–Ernzerhof (PBE) formulation under the generalized gradient approximation (GGA) using first-principles [29–31]. A plane wave base group was applied to consider valence electrons, and ion cores were expressed by means of projected augmented wave (PAW) potentials [32, 33]. Gaussian method permits part occupancies of Kohn–Sham orbitals. The energy variation of less than 0.03 eV is corresponding to the astringent geometric optimization, and energy variation of less than $10^{-6}$ eV indicates self-consistent electronic energy. The value of Fe atom is 3.21 eV under U correction, and the space distance normal to the system plane is 18 Å. The 2 × 2 × 1 Monkhorst–Pack k-point collecting is applied in Brillouin zone integration of a system. At last, the adsorption energies ($E_{adsorption}$) are obtained by $E_{adsorption} = E_{lubricant/substrate} - (E_{lubricant} + E_{substrate})$, where $E_{substrate}$, $E_{lubricant}$, and $E_{lubricant/substrate}$ represent the overall energies of sole substrate, the lubricant molecule, and steady lubricant/substrate system, respectively.

### 2.5 Preparation of surfaces, characterization of adsorption films, and determination of surface energies

In order to remove potential contamination, the steel disks were first washed ultrasonically in n-hexane for 5 min. After drying and cooling, the model lubricant of 0.05 ml was dripped on the cleaned and cooled disk surface. After that, the sample was exposed to RT for 2 h, and an adsorption film was formed on the disk surface. The n-hexane was applied in cleaning residual lubricant on disks. And after drying, the disks underwent infrared (IR) characterization and contact angle measurement.

The IR spectra of adsorption film on steel surface were gotten with the help of the attenuated total reflectance Fourier transform infrared (ATR-FTIR) spectrometer (Nicolet iS10, Thermo Fisher Scientific). The wave number scanning range was 650–4,000 $cm^{-1}$, with the ZnSe attenuated total reflection accessory. The scanning time was 32, and the resolution was 4 $cm^{-1}$.

To figure out the possible surface changes, the surface energies of disks before and after formation of adsorption film were calculated using the Owens–Wendt–Rabel–Kaelble (OWRK) way (Eq. (1)) [34–37]. Water and diiodomethane were selected as the model liquids, and their surface tensions were shown in Table 1. The contact angles of model liquids on measured surfaces were determined by the video measuring device (DSA100, Krüss).

$$\gamma_{\mathrm{L}}\left(1+\cos\theta\right)=2\left(\sqrt{\gamma_{\mathrm{S}}^{\mathrm{D}}\gamma_{\mathrm{L}}^{\mathrm{D}}}+\sqrt{\gamma_{\mathrm{S}}^{\mathrm{P}}\gamma_{\mathrm{L}}^{\mathrm{P}}}\right) \tag{1}$$

where $\gamma_{\mathrm{L}}$ is the total surface energy of liquid; $\theta$ is the contact angle of liquid on solid surface; $\gamma_{\mathrm{S}}^{\mathrm{D}}$ is the surface energy of solid dispersive component; $\gamma_{\mathrm{L}}^{\mathrm{D}}$ is the surface energy of liquid dispersive component; $\gamma_{\mathrm{S}}^{\mathrm{P}}$ is the surface energy of solid polar component; and $\gamma_{\mathrm{L}}^{\mathrm{P}}$ is the surface energy of liquid polar component.

## 3 Results and discussion

### 3.1 Structural characterization

In order to confirm the molecule structures of lubricants, the model lubricants were characterized by the IR spectrometer (Fig. 2). The C–H bond in methyl of n-Nonane displays the absorption peaks at 2,960, 2,873, 1,467, and 1,379 $cm^{-1}$, which represent the stretching vibration and deformation vibration. The stretching vibration of C–H bond in methylene exhibits peaks at 2,925 and 2,856 $cm^{-1}$ [38, 39]; The absorption peaks of 1-Nonene at 3,000–3,100, 970, and 890 $cm^{-1}$ represent the stretching vibration as well as out-of-plane deformation vibration of =C–H. And the

**Table 1** Surface energy and its components of model liquids [34].

| Model liquid | Polar component $\gamma_{\mathrm{L}}^{\mathrm{P}}$ (mJ·m$^{-2}$) | Dispersive component $\gamma_{\mathrm{L}}^{\mathrm{D}}$ (mJ·m$^{-2}$) | Total surface energy $\gamma_{\mathrm{L}}$ (mJ·m$^{-2}$) |
|---|---|---|---|
| Water | 51.00 | 21.80 | 72.80 |
| Diiodomethane | 0 | 50.80 | 50.80 |

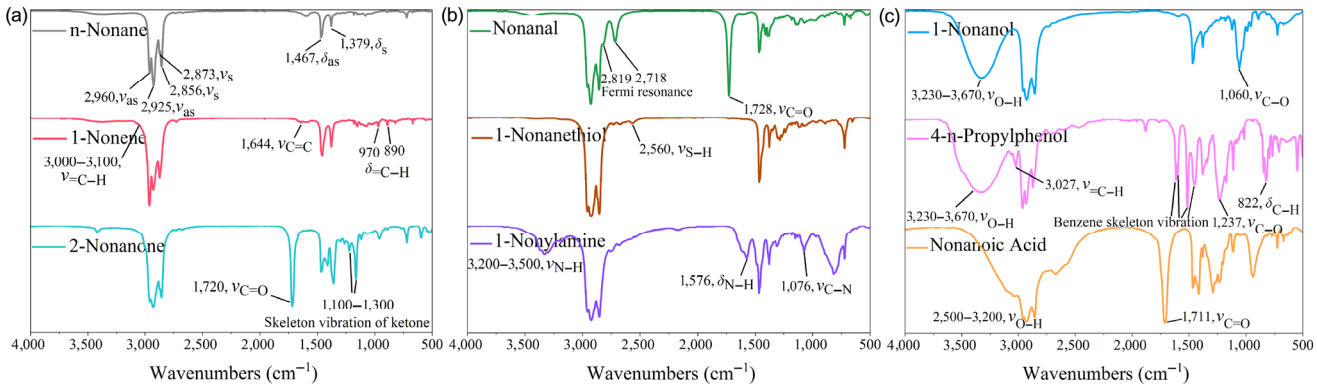


**Fig. 2** FTIR spectra of model lubricant molecules.

stretching vibration occurs for C=C, which produces the absorption at 1,644 $cm^{-1}$; 2-Nonanone displays the absorption at 1,720 $cm^{-1}$ which is from the stretching of C=O and the absorption at 1,100–1,300 $cm^{-1}$ which originates from the skeleton vibration of ketone [38, 39]. Frequency doubling coupling between stretching and deformation vibrations of aldehyde protons in Nonanal brings about Fermi resonance, showing the absorption near 2,819 and 2,718 $cm^{-1}$. The peak at 2,560 $cm^{-1}$ roots in the vibration of S–H in 1-Nonanethiol. The IR outcome of 1-Nonylamine has the absorption peaks at 1,076, 1,576, and 3,200–3,500 $cm^{-1}$ that correspond to the stretching vibration of C–N, the deformation vibration of N–H, and the stretching vibration of N–H, respectively. The absorption peaks of 1-Nonanol at 3,230–3,670 and 1,060 $cm^{-1}$ originate from the stretching vibration of O–H and C–O, respectively [35]. The peaks of 4-n-Propylphenol at 822, 1,237, and 1,500 $cm^{-1}$ are from the deformation vibration of C–H, the stretching vibration of C–O, and the skeleton vibration of benzene ring, respectively. The stretching vibration of O–H in Nonanoic Acid shows the peak at 2,500–3,200 $cm^{-1}$.

### 3.2 Friction test

Relation curves between friction coefficient and time in friction tests of model lubricant molecules are displayed in Fig. 3(a). Friction coefficients of n-Nonane, 1-Nonene, and 2-Nonanone fluctuate widely with time during the whole friction test. However, the friction coefficients of 1-Nonylamine, 1-Nonanol, and 4-n-Propylphenol tend to be stable gradually after the initial running-in process. Nonanal, 1-Nonanethiol, and Nonanoic Acid display steady lubrication performance (Fig. S1 in the Electronic Supplementary Material (ESM)). Figure 3(b) reveals the average friction coefficients in the last 20 min. The wear scar of the steel disk was characterized by means of the three-dimensional (3D) profiler (Fig. 4), and the corresponding wear rate (Fig. 3(c)) was calculated by means of Eq. (2):

$$K = \frac{S \times L}{F \times l} \tag{2}$$

where $K$ ($mm^3 \cdot N^{-1} \cdot m^{-1}$) is the wear rate of disks; $F$ (N) and $l$ (m) are the vertical force and moving length, respectively; $L$ (mm) is the circumference of a circular wear scar; and $S$ ($mm^2$) is the cross-sectional area of wear scar. 1-Nonene shows the highest wear rate, while Nonanal and 1-Nonylamine show the lowest wear rate. Therefore, nine lubricants are divided into three categories based on friction coefficient and wear

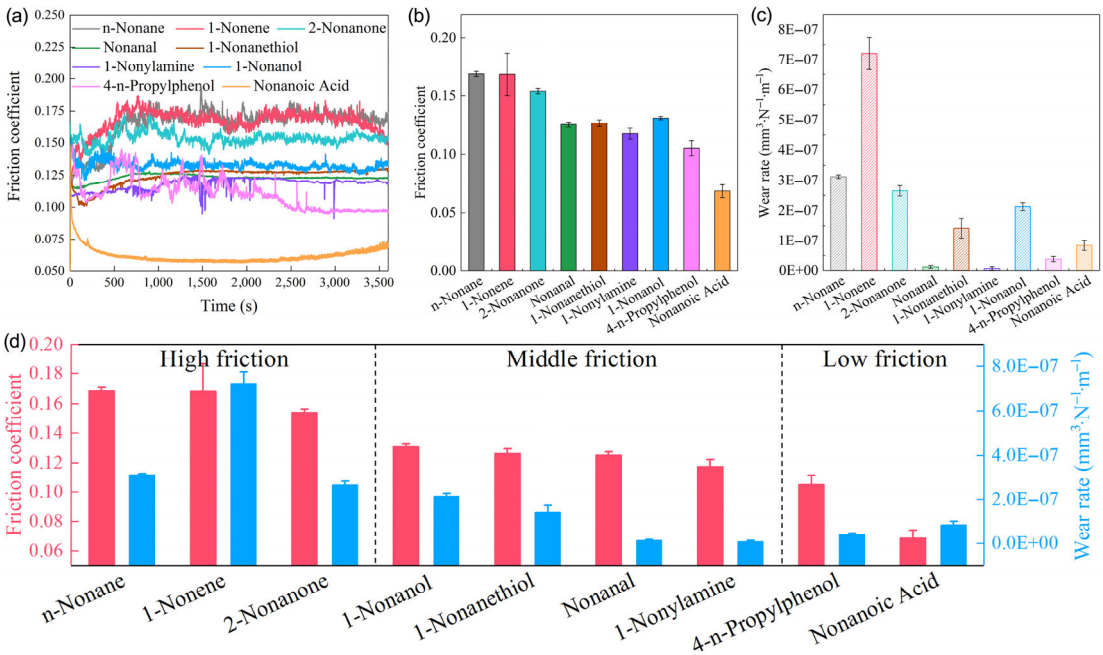


**Fig. 3** (a) Friction coefficients of model lubricant molecules. (b) Average friction coefficients in the last 20 min. (c) Wear rate of the disk after friction tests. (d) Friction coefficient and wear rate of model lubricant (at RT, 90 r·$min^{-1}$, and 10 N).

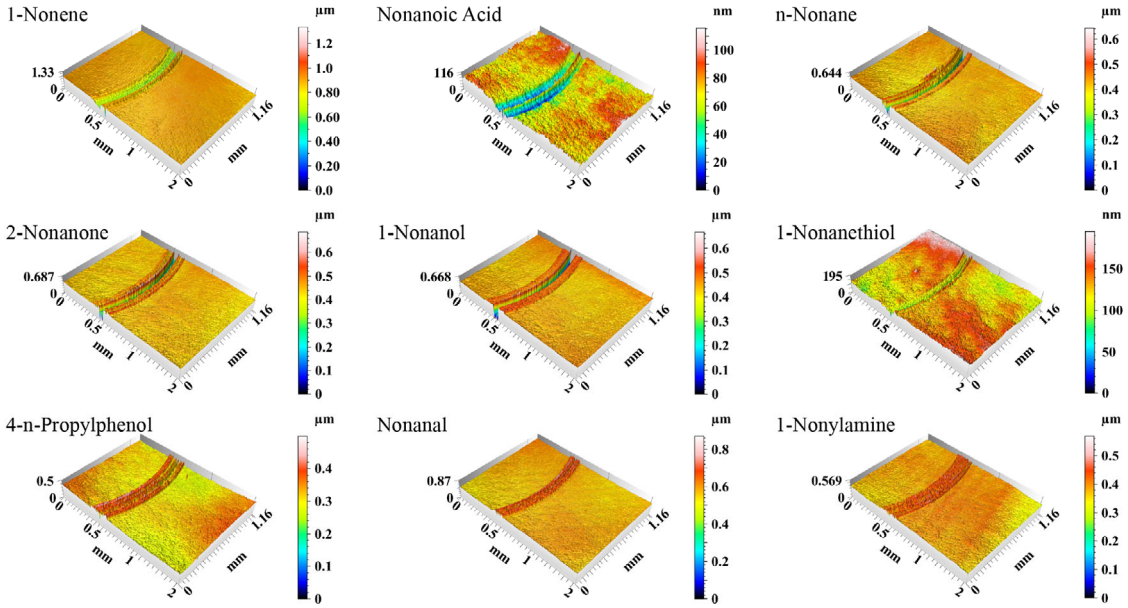


**Fig. 4** 3D morphologies of wear scars lubricated by model lubricants.

rate: High friction includes n-Nonane, 1-Nonene, and 2-Nonanone; middle friction includes 1-Nonanol, 1-Nonanethiol, Nonanal, and 1-Nonylamine; and low friction includes 4-n-Propylphenol and Nonanoic Acid (Fig. 3(d)).

### 3.3 Analysis of the wear scar and debris

Interestingly, there are wear debris rings (WDRs) on disk surface after tribological experiments, and WDRs produced by different model lubricants display different morphologies and distributions (Figs. 5(a) and 5(b)). In order to study the composition of WDRs, n-Nonane with the most diverse WDRs was used as an example to characterize its WDRs by the optical microscopy and Raman spectroscopy (Figs. 5(d) and 5(e), respectively). By observing the morphologies of different positions of WDRs, it can be found that the wear debris of outer ring shows the smaller size. It can be found from Fig. 5(e) that different positions of WDRs show similar Raman spectra, corresponding to the absorption peaks of iron oxide ($Fe_3O_4$ as the reference). This indicates that the whole friction process is dominated by oxidative wear, which causes the friction coefficient to fluctuate violently (Fig. 3(a)) [40]. In addition, the D bands near 1,380 $cm^{-1}$ and G bands at 1,594 $cm^{-1}$ are obvious in the Raman spectroscopy result of wear debris, indicating that there are much carbonous material in wear debris [41, 42]. Furthermore, the large Raman shift of G band near 1,594 $cm^{-1}$ proves that carbonous matter is highly disordered [43, 44]. Because of hydrogenated carbon in wear debris, the stretching of $CH_x$ can bring about the absorption around 2,904 $cm^{-1}$ [40, 44].

It can be found that the model lubricants belonging to high friction produce more obvious WDRs in the friction test. The explanation for this phenomenon is as follows: Main components of WDRs are iron oxide and carbonous material. Lubricants belonging to high friction correspond to high frictional force/shear stress, which is beneficial to formation of iron oxide and tribochemical reaction of model lubricant to produce carbonous material. The lubricants belonging to high friction correspond to high wear rate, which also makes WDRs more obvious. WDRs of model lubricants belonging to middle friction are not obvious, and there are no WDRs on disk surface after tribological experiment of lubricants belonging to low friction.

After friction tests, disks were investigated by the SEM–EDS to evaluate wear scars (Fig. 6). The wear mechanisms of n-Nonane, 1-Nonene, and 2-Nonanone belonging to high friction are severe ploughing wear, corresponding to large wear rates. The smoother wear scars of 1-Nonanol, Nonanal, 1-Nonanethiol, and 1-Nonylamine belonging to middle friction show slight ploughing groove and lower wear rates. The

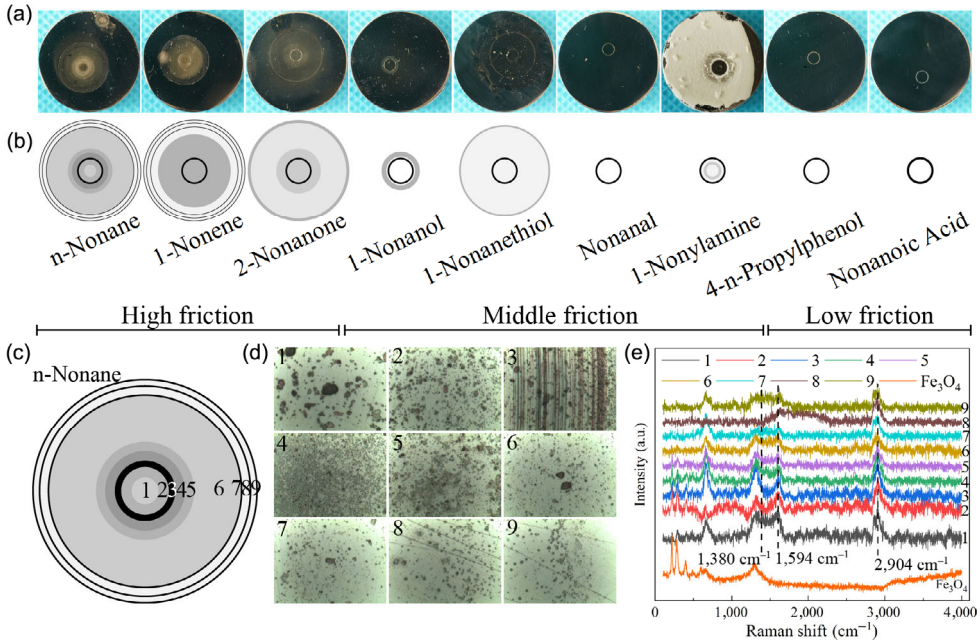


**Fig. 5** (a) Photographs of WDRs formed on the disk surface after tribological experiment. (b) Schematic diagrams of WDRs. (c) Schematic diagram of WDRs formed on the disk surface after friction test of n-Nonane. (d) Optical micrographs and (e) Raman spectra of different positions of WDRs marked in (c).

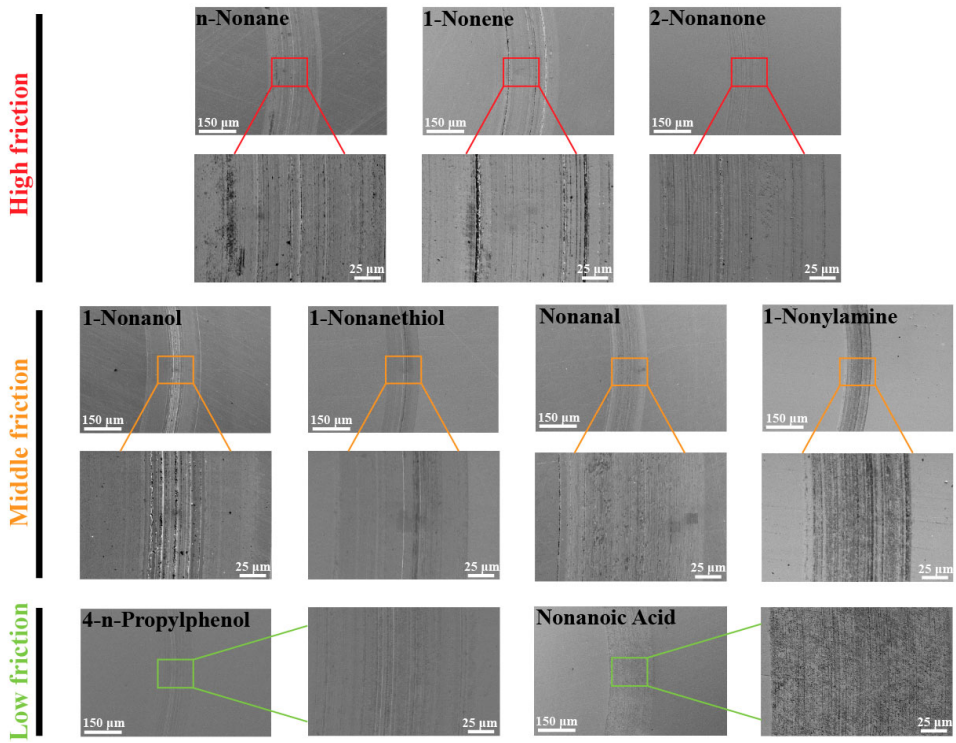


**Fig. 6** SEM images of wear scars (magnifications: 200× and 2,000×).

tribofilm of 1-Nonylamine containing N element (Table 2) can account for its small wear rate. The wear mechanisms of Nonanoic Acid and 4-n-Propylphenol belonging to low friction are slight ploughing wear. In addition, there are plenty of granular debris on the wear scar of Nonanoic Acid. The granular debris is evenly distributed on the whole contact interface, which can significantly reduce the direct contact of

**Table 2** EDS data for wear scars of model lubricants.

| Chemistry | C (at%) | O (at%) | Cr (at%) | Fe (at%) | N (at%) | S (at%) |
|---|---|---|---|---|---|---|
| n-Nonane | 14.0 | 1.7 | 1.6 | 82.7 | — | — |
| 1-Nonene | 26.8 | 14.0 | 3.4 | 55.7 | — | — |
| 2-Nonanone | 13.8 | 2.6 | 1.6 | 82.1 | — | — |
| Nonanal | 12.2 | 4.3 | 1.6 | 81.9 | — | — |
| 1-Nonanethiol | 24.1 | 7.2 | 3.8 | 58.2 | — | 6.7 |
| 1-Nonylamine | 12.2 | 6.1 | 1.6 | 79.7 | 0.3 | — |
| 1-Nonanol | 23.8 | 20.0 | 3.0 | 53.2 | — | — |
| 4-n-Propylphenol | 12.7 | 7.4 | 1.5 | 78.4 | — | — |
| Nonanoic Acid | 15.3 | 1.3 | 1.6 | 81.8 | — | — |

friction pair in the friction process and play a good role in sharing the contact stress, bringing a small wear rate.

### 3.4 Lubrication mechanism for Nonanoic Acid of excellent tribological properties

#### *3.4.1 Determination of lubrication regime for Nonanoic Acid*

Considering friction coefficient and wear rate, Nonanoic Acid has superior tribological properties than those of other model lubricants. In order to figure out the action mechanism of functional groups on tribological properties of lubricants, it is crucial to explore the lubrication mechanism of Nonanoic Acid. Therefore, a sequence of experiments were performed to determine its lubrication regime under experimental conditions (RT, 90 r·min$^{-1}$, and 10 N). Figure 7(a) shows the friction coefficients obtained with five velocities, 30, 60, 90, 120, and 150 r·min$^{-1}$. The friction coefficients fluctuate violently with time at low rotational velocities (30 and 60 r·min$^{-1}$), but the friction coefficients become more stable along with the increase of rotating speed. Mean friction coefficients of the whole test under various rotational velocities as a function of $\eta\omega/p$ are shown (Fig. 7(b)), where $\eta$ is the lubricant viscosity (N·m$^{-2}$·s), $\omega$ is the angular velocity (s$^{-1}$), and $p$ is the applied pressure (N·m$^{-2}$). And the influence of rubbing heat on lubricant viscosity is negligible. The results show that the friction coefficient decreases first, and then increases with the increase of rotating speed. The lubrication regime can be divided into boundary lubrication, mixed lubrication, and hydrodynamic lubrication based on the variation law of the Stribeck curve and the value of friction coefficient [45]. The Stribeck curve (friction coefficient vs. $\eta\omega/p$) shown in Fig. 7(b) indicates that the lubrication regime with velocity of 90 r·min$^{-1}$ lies in mixed lubrication regime. It should be noted that $p$ used in the calculation of $\eta\omega/p$ is the maximum Hertz contact stress, and the

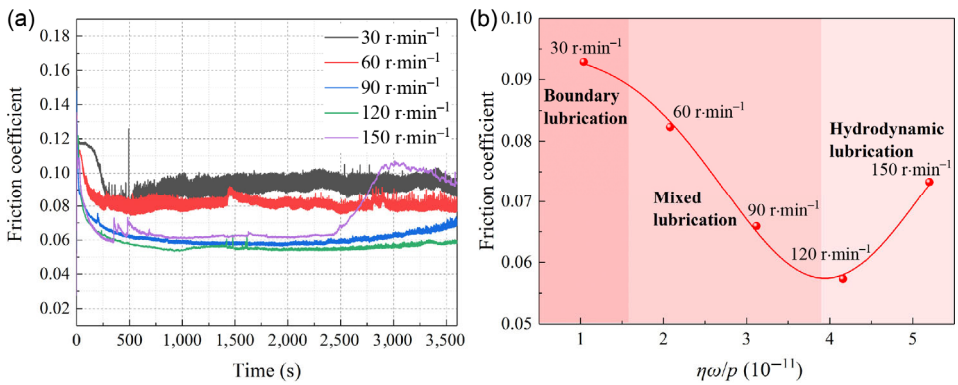


**Fig. 7** (a) Friction coefficients of Nonanoic Acid under various rotational velocities. (b) Mean friction coefficients of the whole test under various rotational velocities (at RT and 10 N).

actual contact pressure will decrease due to the wear in the friction experiment, resulting in larger $\eta\omega/p$. But it can be found from the Stribeck curve that the lubrication regime is still in the mixed lubrication regime. The fluid film and tribofilm are coexistent in mixed lubrication regime, which can bring excellent tribological properties [46].

### 3.4.2 *Analysis of the wear scar and debris from friction test of Nonanoic Acid*

The Raman and XPS analyses to the wear scar were carried out for ascertaining the composition of the tribofilm (Figs. 8(a) and 8(d)). The results of the Raman spectra show that the main component of the tribofilm is $Fe_3O_4$, and the Raman absorptions at 1,389, 1,582, and 2,901 $cm^{-1}$ are ascribed to carbonaceous matter in the tribofilm. The XPS outcomes of wear scar were displayed in Fig. 8(d) to study the valence states of different elements. The XPS signals of Fe 2p (723.1 eV) and O 1s (530.5 eV) indicate the presence of $Fe_3O_4$ [47]. The peaks of Fe 2p (713.4 and 709.8 eV) and O 1s (533.0 and 531.2 eV) can be attributed to FeOOH and Fe(OH)O [48]. The binding energies of C 1s around 284.8, 285.6, and 289.2 eV probably belong to C–C, C–O, and C=O, individually. This is possibly due to carbonaceous material produced in the process of frictional experiment [41]. It can be found from Figs. 8(b) and 8(c) that compared with blank steel, the elastic modulus and hardness of wear scar are decreased, which also proves the formation of iron oxide and carbonaceous matter in tribofilm.

The analysis of wear debris can also reflect the composition of tribofilm from the side view. Thus, the morphologies of the wear debris particles collected in tribological experiment of Nonanoic Acid were studied by the TEM (Fig. 9), and the particles exhibit granular appearance. The lattice fringe spacing in the high-resolution transmission electron microscopy (HRTEM) micrograph of debris particles (Fig. 9(c)) is approximately 0.25 nm, which originates from the lattice spacing of the crystal face (311) for $Fe_3O_4$ [49, 50]. Figure 9(d) is the scanning transmission electron microscopy (STEM) image of wear debris. By the mapping analysis (Figs. 9(e)–9(g)), C, O, and Fe elements were equably distributed in wear debris. This result conforms to the conclusion got from the XPS and Raman outcomes of tribofilm on wear scar. In addition, it can be found from Fig. 9(b) that a small amount of graphene nanoribbon showing a lattice distance of 0.34 nm, which comes from the crystal face (002) of graphene [51], can be observed at the edge of the debris particle. This outcome is in accordance with the existence of carbonaceous matter in tribofilm obtained from the Raman and XPS analyses. The graphene nanoribbon also provides favorable condition

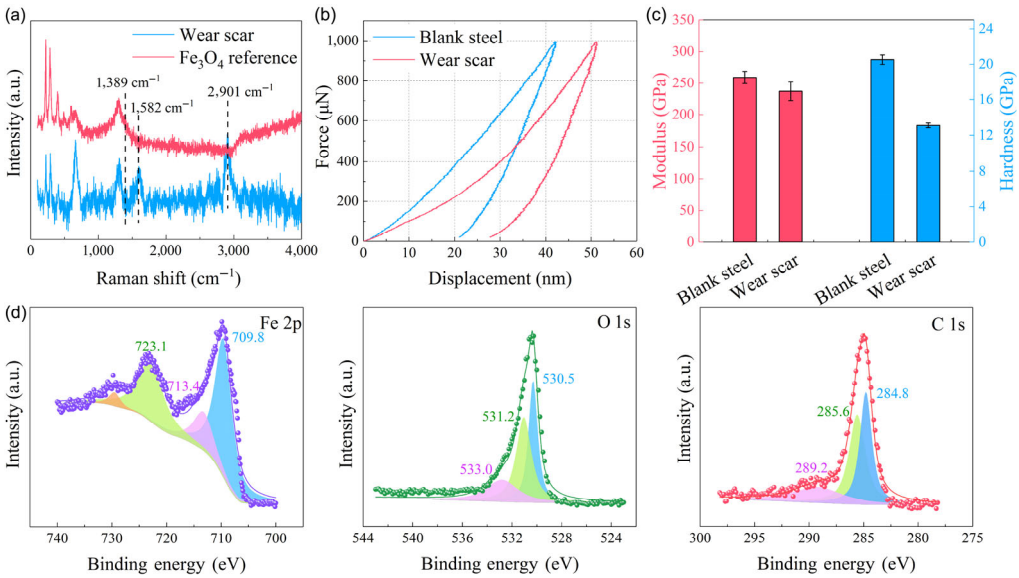


**Fig. 8** Characterizations of wear scar obtained from the friction test of Nonanoic Acid (at RT, 90 $r \cdot min^{-1}$, and 10 N). (a) Raman spectra of wear scar and $Fe_3O_4$ reference. (b) Force–displacement curves of blank steel and wear scar. (c) Elastic moduli and hardnesses of blank steel and wear scar. (d) XPS outcomes of C 1s, O 1s, and Fe 2p of wear scar.

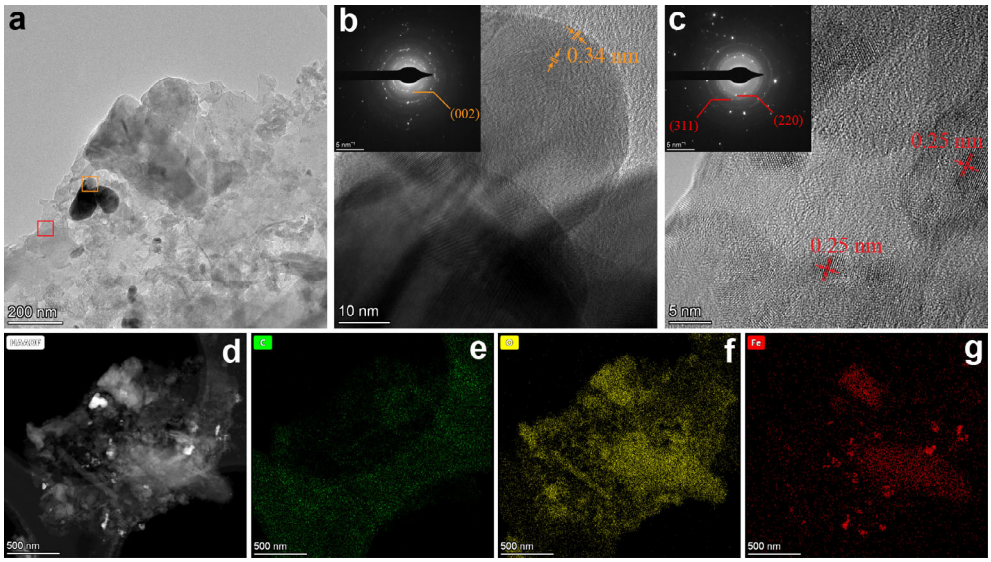


**Fig. 9** (a) TEM micrograph of wear debris collected in tribological experiment of Nonanoic Acid (at RT, 90 r·min$^{-1}$, and 10 N). (b) TEM micrograph of the orange square region in (a) and selected area electron diffraction (SAED) pattern (the inset). (c) HRTEM micrograph of the red square region in (a) and SAED pattern (the inset). (d) High-angle annular dark-field scanning transmission electron microscopy (HAADF-STEM) image of wear debris and relevant elemental distribution of (e) C, (f) O, and (g) Fe.

for low friction and wear of Nonanoic Acid in friction process [43].

### 3.4.3 *Lubrication mechanism of Nonanoic Acid*

Combining the above findings about friction test of Nonanoic Acid, the lubrication mechanism of Nonanoic Acid is probed. The Stribeck curve indicates that the lubrication regime with velocity of 90 r·min$^{-1}$ of Nonanoic Acid is in the mixed lubrication regime. Nonanoic Acid molecules can be adsorbed on the substrate surface and form a steady fluid film. Under the condition of friction, interaction between Nonanoic Acid molecules and iron substrate triggers complex tribochemical reactions, producing graphene nanoribbon, $Fe_3O_4$ nanoparticles, and additional carbonaceous matter. And these become the main components of the tribofilm. The fluid film and tribofilm together bring low friction coefficient and wear rate for Nonanoic Acid.

## 3.5 Action mechanism investigation of functional groups on friction coefficient and wear rate

Based on the findings for the lubrication mechanism of Nonanoic Acid, it can be concluded that its excellent lubrication performance comes from the coexistence of fluid film and tribofilm. And both fluid film and tribofilm originate from the interaction between lubricant molecules and steel substrates. Therefore, the adsorption of lubricant molecules on steel substrates has become the primary concern to clarify the action mechanism of functional groups on lubrication performance of lubricants. Furthermore, the adsorption energies of nine kinds of lubricant molecules on steel surface were calculated by DFT (Fig. 10(a)). The outcome in Fig. 10(b) indicates that the molecule with higher adsorption energy possesses smaller friction coefficient. The adsorption energy is calculated by subtracting the respective energies before adsorption from the total energy of the system after the lubricant molecules adsorbed on the substrate surface. The larger adsorption energy means that adsorbed system is more stable, and the lubricant molecules are more apt to adsorb on the substrate surface. In the dynamic process of relative motion, these lubricant molecules can produce a film on metal surface. The long chain tail is normal to metal surface, and head group adheres to surface [17]. Because of the van der Waals force among long chain tails of adsorbed lubricants and the dipole–dipole interaction among the contiguous polar groups, these molecules form a vertically tightly-packed monolayer film. And the friction reduction is usually attributed

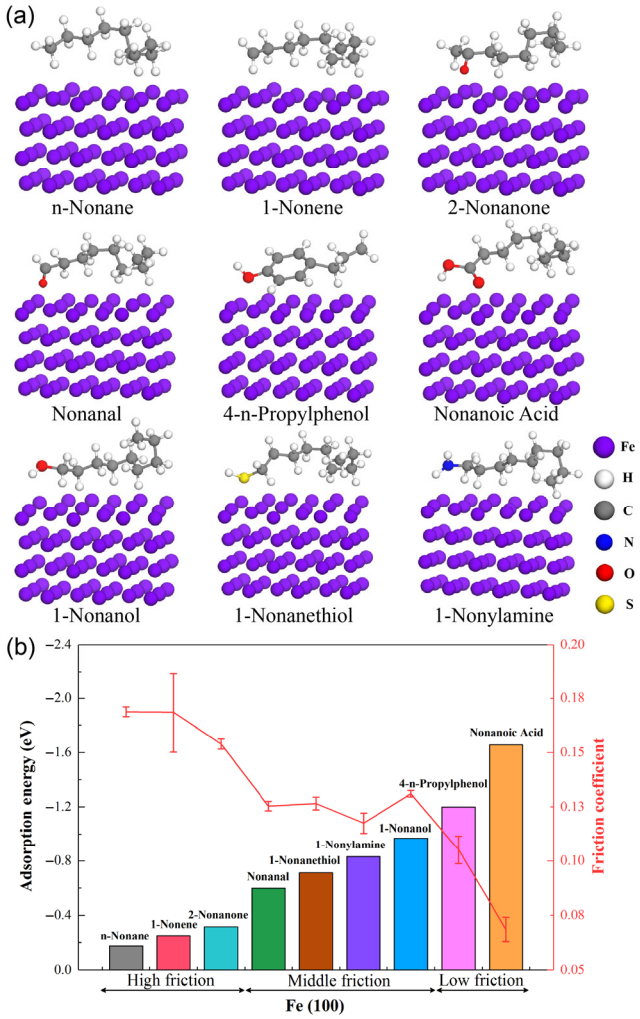


**Fig. 10** (a) Model lubricant molecules and Fe substrate employed in DFT calculations. (b) Adsorption energies and friction coefficients (at RT, 90 r·min$^{-1}$, and 10 N) of nine kinds of lubricant molecules on steel surface.

to the building of monolayer on friction interface [16, 52]. The film is very firm and able to bear large load owing to accumulation of van der Waals forces among molecules [8]. Under action of load and shear stress, the incompressible adsorption layer is easy to slide between opposite polar groups, resulting in the reduction of friction and adhesion [8]. Therefore, the molecules with higher adsorption energy are more likely to be adsorbed on substrates and produce a stable monolayer adsorption layer, reducing friction coefficient.

The lubricant molecule forms an adsorption film on the steel substrate, which is bound to change the physicochemical properties of the steel surface. Therefore, Fig. 11(a) displays the ATR-FTIR spectra of disks with adsorption film. The outcomes indicate that all the lubricant molecules form adsorption films on the surface of steel substrates. The absorption peaks near 2,900 cm$^{-1}$ originate from the stretching vibration of C–H bond. The signal near 3,200–3,500 cm$^{-1}$ is from the stretching vibrations of O–H and N–H, and the absorption at 1,700 cm$^{-1}$ comes from the stretching vibration of C=O. The adsorption film changes physicochemical characters of substrate surface, and the surface energies of the samples after forming the adsorption films at RT is shown in Fig. 11(b). The surface energy of blank steel (37.1 mJ·m$^{-2}$) is less than those of the samples with adsorption films. The results of surface energy also show that all the model lubricants can form adsorption films on the steel surface at RT.

The contact angle measurements (Fig. S2 in the ESM) were conducted to calculate the surface energies after the adsorption film formation. The outcome in Fig. 11(b) indicates that the molecule with higher surface energy tends to possess smaller wear rate. The surface energy of the lubricant belonging to high friction is lower than those of middle friction and low friction on the whole, while the wear rate of the lubricant in high friction is higher than that of middle friction and low friction. And it also can be found that Nonanal, 1-Nonylamine, 4-n-Propylphenol, and Nonanoic Acid with the higher surface energies display smaller wear rates in friction test. The surface energy of Nonanoic Acid is lower than those of 4-n-Propylphenol and 1-Nonylamine, and the wear rate of Nonanoic Acid is higher than those of 4-n-Propylphenol and 1-Nonylamine, which is consistent with the above law. Surface energy is defined as the excess energy of surface particles relative to internal particles, and the matter with higher energy is more unstable [53]. Therefore, the lubricant molecules in the adsorption film with higher surface energy may be more chemically unstable. In addition, the wear is in connection with film-forming ability of lubricant molecules on the friction interface. The lubricant molecules in the adsorption film with large surface energy may be more prone to tribochemical reaction to form tribofilm under friction condition, which prevents direct contact of friction pair and leads to low wear rate. In addition, it should be pointed out that the wear rate in the friction test must

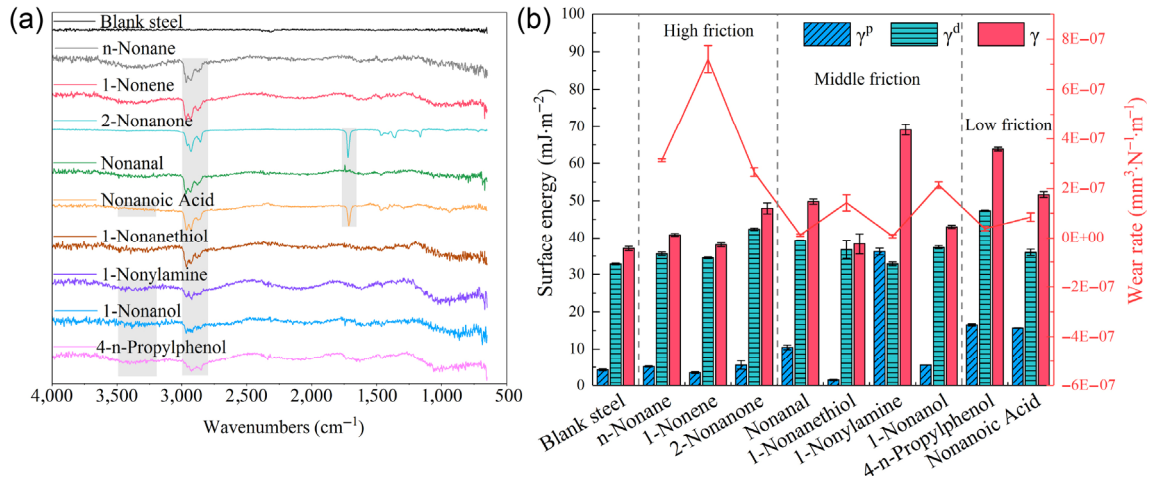


**Fig. 11** (a) ATR-FTIR spectra of disks with adsorption films. (b) Surface energies of disks with adsorption films and wear rates (at RT, 90 r·min$^{-1}$, and 10 N). $\gamma^p$ is the surface energy of polar component; $\gamma^d$ is the surface energy of dispersive component; and $\gamma$ is the total surface energy.

be affected by other factors except surface energy, but this study only gives a reasonable explanation for the relationship between surface energy and wear rate and does not consider more about other influence factors.

### 3.6 Discussions

In view of the above experimental results and previous literature reports, the action mechanism of different functional groups on lubrication performances of lubricants is summarized, and Fig. 12 displays the mechanism diagram. Various functional groups make lubricant molecules show different adsorption energies and surface energies. Due to head groups with various functional groups, lubricant molecules

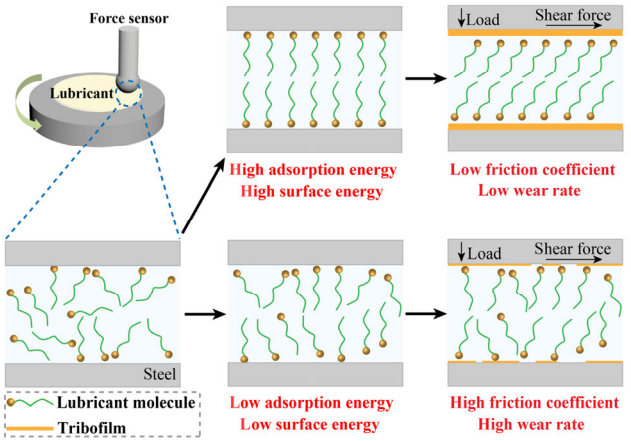


**Fig. 12** Action mechanism of functional groups on lubrication performances of lubricants.

on sliding surface would form adhesive bonding of different intensity with the steel substrate. And the lubricant with low friction coefficient in the friction test corresponds to high adsorption energy in DFT calculations. The lubricant molecules with higher adsorption energy are more likely to adsorb on the substrate surface and form a vertical monolayer. Under the action of load and shear force, the hydrocarbon tail easily slips between opposite polar groups, resulting in the decrease of friction coefficient. During the friction process, the adsorbed monolayer will inevitably be destroyed, but the lubricant molecules with higher adsorption energy can be more quickly adsorbed on the substrate surface to maintain the regular molecular brush structure, so that the friction coefficient is kept low throughout the whole friction process. However, the interaction between substrates and lubricant molecules with low adsorption energies is weak. The arrangement of lubricant molecules between sliding interfaces is disordered, resulting in high friction coefficient [12]. Furthermore, Fig. 13 indicates that the adsorption energies of lubricant molecules on steel surface positively correlate the surface energies after the adsorption film formation. The lubricant molecules which form adsorption film with high surface energy on the steel surface show low wear rate (Fig. 11(b)). Based on this experimental fact, it is inferred that the lubricant molecules in the adsorption film with higher surface energy are more likely to conduct tribochemical

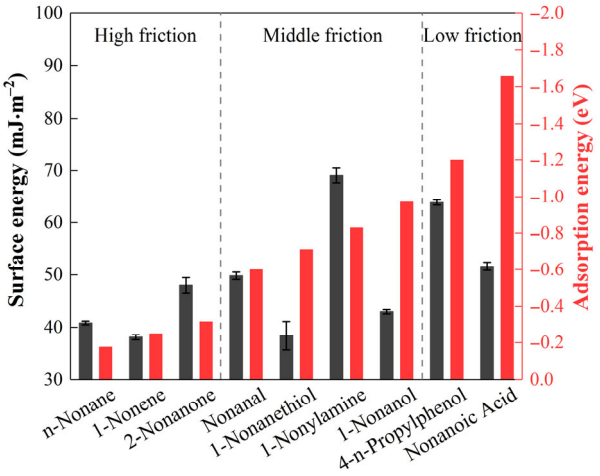


**Fig. 13** Relationship between adsorption energies of lubricant molecules on steel surface and surface energies after the adsorption film formation.

reaction in the friction process and form protective tribofilm, which leads to low wear rate. On the contrary, the lubricant molecules in the adsorption film with low surface energy cannot form an effectively protective tribofilm during friction, resulting in high wear rate.

## 4 Conclusions

1) Nine organic compounds were utilized as model lubricants to explore the effect of functional groups on tribological properties. Nine lubricants could be divided into three categories based on friction coefficients and wear rates: high friction; middle friction; and low friction.

2) There were WDRs on the disk surface after tribological experiment, and the model lubricant with higher friction coefficient produced more obvious WDRs in the friction test. The Raman spectra showed that main components of WDRs were iron oxide and carbonous material. In addition, the wear scars of disks were analyzed by the SEM–EDS to investigate the wear mechanisms.

3) Nonanoic Acid with carboxyl showed the best lubrication properties, and the mechanism for the excellent tribological properties of Nonanoic Acid was explored. The Stribeck curve indicated that its lubrication regime was in mixed lubrication regime, where fluid film and tribofilm were coexistent. The Raman, XPS, and TEM analyses indicated that graphene nanoribbon, $Fe_3O_4$ nanoparticles, and additional carbonaceous matter composed tribofilm.

4) To investigate the action mechanism of molecular structure on tribological properties, adsorption energies of lubricant molecules on steel surface and surface energies after the adsorption film formation were obtained separately by DFT simulations and contact angle tests. Various functional groups make lubricant molecules show different adsorption energies and surface energies. The outcome indicated that higher adsorption energy corresponded to smaller friction coefficient and higher surface energy corresponded to smaller wear rate. Moreover, adsorption energies positively correlated surface energies.

5) The action mechanism of different functional groups on lubrication performance of lubricants is summarized as follows. Various functional groups make lubricant molecules show different adsorption energies and surface energies. The lubricant molecules with higher adsorption energy are more likely to adsorb on the substrate surface and form a vertical monolayer. Under the action of load and shear force, the lubricant molecules with higher adsorption energy can still maintain the regular molecular brush structure, so that the friction coefficient is kept low throughout the whole friction process. However, the interaction between substrates and lubricant molecules with low adsorption energy is weak. The disordered arrangement of lubricant molecules results in high friction coefficient. Besides that, it is inferred that lubricant molecules in the adsorption layer with higher surface energy are more likely to conduct tribochemical reaction in the friction process and form protective tribofilm, which leads to low wear rate. In brief, the lubricants with high adsorption energies and surface energies show low friction coefficients and wear rates. This study has guiding significance for the development and utilization of novel lubricants and additives.

## Acknowledgements

The authors are grateful for the financial support from Youth Innovation Promotion Association, Chinese Academy of Sciences (2021422) and Lanzhou Institute of Chemical Physics (LICP) Cooperation Foundation for Young Scholars (HZJJ20-06).

## Declaration of competing interest

The authors have no competing interests to declare that are relevant to the content of this article.

**Electronic Supplementary Material** Supplementary material is available in the online version of this article at https://doi.org/10.1007/s40544-022-0630-9.



## References

[1] Holmberg K, Erdemir A. Influence of tribology on global energy consumption, costs and emissions. *Friction* **5**(3): 263–284 (2017)

[2] Guo H, Iglesias P. Tribological behavior of ammonium-based protic ionic liquid as lubricant additive. *Friction* **9**(1): 169–178 (2021)

[3] Ouyang C K, Bai P P, Wen X L, Zhang X J, Meng Y G, Ma L R, Tian Y. Effects of conformational entropy on antiwear performances of organic friction modifiers. *Tribol Int* **156**: 106848 (2021)

[4] Holmberg K, Andersson P, Erdemir A. Global energy consumption due to friction in passenger cars. *Tribol Int* **47**: 221–234 (2012)

[5] Zhang S W. Green tribology: Fundamentals and future development. *Friction* **1**(2): 186–194 (2013)

[6] Kuwahara T, Romero P A, Makowski S, Weihnacht V, Moras G, Moseler M. Mechano-chemical decomposition of organic friction modifiers with multiple reactive centres induces superlubricity of ta-C. *Nat Commun* **10**: 151 (2019)

[7] Ewen J P, Gattinoni C, Morgan N, Spikes H A, Dini D. Nonequilibrium molecular dynamics simulations of organic friction modifiers adsorbed on iron oxide surfaces. *Langmuir* **32**(18): 4450–4463 (2016)

[8] Cyriac F, Tee X Y, Poornachary S K, Chow P S. Influence of structural factors on the tribological performance of organic friction modifiers. *Friction* **9**(2): 380–400 (2021)

[9] Fry B M, Chui M Y, Moody G, Wong J S S. Interactions between organic friction modifier additives. *Tribol Int* **151**: 106438 (2020)

[10] Guegan J, Southby M, Spikes H. Friction modifier additives, synergies and antagonisms. *Tribol Lett* **67**(3): 83 (2019)

[11] Tang Z L, Li S H. A review of recent developments of friction modifiers for liquid lubricants (2007–present). *Curr Opin Solid State Mater Sci* **18**(3): 119–139 (2014)

[12] Shi J Q, Zhou Q, Sun K, Liu G Q, Zhou F. Understanding adsorption behaviors of organic friction modifiers on hydroxylated $SiO_2$ (001) surfaces: Effects of molecular polarity and temperature. *Langmuir* **36**(29): 8543–8553 (2020)

[13] Spikes H. Friction modifier additives. *Tribol Lett* **60**(1): 5(2015)

[14] Ratoi M, Niste V B, Alghawel H, Suen Y F, Nelson K. The impact of organic friction modifiers on engine oil tribofilms. *RSC Adv* **4**(9): 4278–4285 (2014)

[15] Fry B M, Moody G, Spikes H A, Wong J S S. Adsorption of organic friction modifier additives. *Langmuir* **36**(5): 1147–1155 (2020)

[16] Jahanmir S, Beltzer M. Effect of additive molecular structure on friction coefficient and adsorption. *J Tribol* **108**(1): 109–116 (1986)

[17] Jahanmir S. Chain length effects in boundary lubrication. *Wear* **102**(4): 331–349 (1985)

[18] Shi J Q, Zhang M, Liu J X, Liu G Q, Zhou F. Molecular dynamics simulations of adsorption behavior of organic friction modifiers on hydrophilic silica surfaces under the effects of surface coverage and contact pressure. *Tribol Int* **156**: 106826 (2021)

[19] Vuorte M, Vierros S, Kuitunen S, Sammalkorpi M. Adsorption of impurities in vegetable oil: A molecular modelling study. *J Colloid Interface Sci* **571**: 55–65 (2020)

[20] Zhou P, Hou J, Yan Y G, Wang J Q. The effect of surfactant adsorption on surface wettability and flow resistance in slit nanopore: A molecular dynamics study. *J Colloid Interface Sci* **513**: 379–388 (2018)

[21] Pominov A, Müller-Hillebrand J, Träg J, Zahn D. Interaction models and molecular simulation systems of steel–organic friction modifier interfaces. *Tribol Lett* **69**(1): 14 (2021)

[22] Tatsumi G, Ratoi M, Shitara Y, Sakamoto K, Mellor B G. Effect of organic friction modifiers on lubrication of PEEK–steel contact. *Tribol Int* **151**: 106513 (2020)

[23] Piras F M, Rossi A, Spencer N D. Growth of tribological films: *In situ* characterization based on attenuated total reflection infrared spectroscopy. *Langmuir* **18**(17): 6606–6613 (2002)

[24] Beltzer M. Assessing adsorption of conventional friction modifying molecules by relative contact potential difference measurements. *J Tribol* **114**(4): 675–682 (1992)

[25] Campen S, Green J H, Lamb G D, Spikes H A. *In situ* study of model organic friction modifiers using liquid cell AFM; saturated and mono-unsaturated carboxylic acids. *Tribol Lett* **57**(2): 18 (2015)

[26] Choo J H, Forrest A K, Spikes H A. Influence of organic friction modifier on liquid slip: A new mechanism of organic friction modifier action. *Tribol Lett* **27**(2): 239–244 (2007)

[27] Onumata Y, Zhao H Y, Wang C, Morina A, Neville A. Interactive effect between organic friction modifiers and additives on friction at metal pushing V-belt CVT components. *Tribol Trans* **61**(3): 474–481 (2018)

[28] Okubo H, Watanabe S, Tadokoro C, Sasaki S. Effects of concentration of zinc dialkyldithiophosphate on the tribological properties of tetrahedral amorphous carbon films in presence of organic friction modifiers. *Tribol Int* **94**: 446–457 (2016)

[29] Kresse G, Furthmüller J. Efficiency of *ab-initio* total energy calculations for metals and semiconductors using a plane-wave basis set. *Comput Mater Sci* **6**(1): 15–50 (1996)

[30] Kresse G, Furthmüller J. Efficient iterative schemes for *ab initio* total-energy calculations using a plane-wave basis set. *Phys Rev B* **54**(16): 11169–11186 (1996)

[31] Perdew J P, Burke K, Ernzerhof M. Generalized gradient approximation made simple. *Phys Rev Lett* **77**(18): 3865–3868 (1996)

[32] Kresse G, Joubert D. From ultrasoft pseudopotentials to the projector augmented-wave method. *Phys Rev B* **59**(3): 1758–1775 (1999)

[33] Blöchl P E. Projector augmented-wave method. *Phys Rev B* **50**(24): 17953–17979 (1994)

[34] Kalin M, Polajnar M. The correlation between the surface energy, the contact angle and the spreading parameter, and their relevance for the wetting behaviour of DLC with lubricating oils. *Tribol Int* **66**: 225–233 (2013)

[35] Kus M, Kalin M. Additive chemical structure and its effect on the wetting behaviour of oil at 100 °C. *Appl Surf Sci* **506**: 145020 (2020)

[36] Han Y Y, Qiao D, Zhang S W, Feng D P. Influence of phosphate and phosphonate ionic liquid structures on lubrication for different alloys (Mg, Al, Cu). *Tribol Int* **114**: 469–477 (2017)

[37] Ba Z W, Huang G W, Qiao D, Feng D P. Experimental and calculation studies on the relationship between the hygroscopic behavior and lubrication properties of ionic liquids. *Appl Surf Sci* **529**: 147031 (2020)

[38] Kumar S, Panigrahi P, Saw R K, Mandal A. Interfacial interaction of cationic surfactants and its effect on wettability alteration of oil-wet carbonate rock. *Energy Fuels* **30**(4): 2846–2857 (2016)

[39] Kumar S, Mandal A. Studies on interfacial behavior and wettability change phenomena by ionic and nonionic surfactants in presence of alkalis and salt for enhanced oil recovery. *Appl Surf Sci* **372**: 42–51 (2016)

[40] Xu X, Xu Z B, Sun J F, Tang G B, Su F H. *In situ* synthesizing carbon-based film by tribo-induced catalytic degradation of poly-α-olefin oil for reducing friction and wear. *Langmuir* **36**(35): 10555–10564 (2020)

[41] Yu H X, Chen H J, Zheng Z W, Ba Z W, Qiao D, Feng D P, Gong Z B, Dong G J. Transformation mechanism between the frictional interface under dioctyl sebacate lubrication. *Tribol Int* **155**: 106745 (2021)

[42] Wu H X, Khan A M, Johnson B, Sasikumar K, Chung Y W, Wang Q J. Formation and nature of carbon-containing tribofilms. *ACS Appl Mater Interfaces* **11**(17): 16139–16146 (2019)

[43] Erdemir A, Ramirez G, Eryilmaz O L, Narayanan B, Liao Y F, Kamath G, Sankaranarayanan S K R S. Carbon-based tribofilms from lubricating oils. *Nature* **536**(7614): 67–71 (2016)

[44] Ferrari A C, Robertson J. Resonant Raman spectroscopy of disordered, amorphous, and diamondlike carbon. *Phys Rev B* **64**(7): 075414 (2001)

[45] Wen S Z, Huang P. Properties of lubricants. In: *Principles of Tribology*, 2nd edn. Wen S Z, Huang P, Eds. Beijing: Tsinghua University Press, 2017: 1–21.

[46] Wen S Z, Huang P. Lubrication failure and mixed lubrication. In: *Principles of Tribology*, 2nd edn. Wen S Z, Huang P, Eds. Beijing: Tsinghua University Press, 2017: 190–208.

[47] Huang G W, Yu Q L, Ma Z F, Cai M R, Liu W M. Probing the lubricating mechanism of oil-soluble ionic liquids additives. *Tribol Int* **107**: 152–162 (2017)

[48] Ba Z W, Han Y Y, Qiao D, Feng D P, Huang G W. Composite nanoparticles based on hydrotalcite as high performance lubricant additives. *Ind Eng Chem Res* **57**(45): 15225–15233 (2018)

[49] Sun J K, Zan P, Yang X J, Ye L, Zhao L J. Room-temperature synthesis of $Fe_3O_4$/Fe–carbon nanocomposites

with Fe–carbon double conductive network as supercapacitor. *Electrochimica Acta* **215**: 483–491 (2016)

[50] Li Y L, Duan W Y, Lu X G, Yang S, Wen X X. Synthesis of strawberry-like $Fe_3O_4$@$SiO_2$@Ag composite colloidal particles for constructing responsive photonic crystals. *Opt Mater* **94**: 423–429 (2019)

[51] Hu J, Xu Z L, Li X Y, Liang S J, Chen Y M, Lyu L L, Yao H M, Lu Z G, Zhou L M. Partially graphitic hierarchical porous carbon nanofiber for high performance supercapacitors and lithium ion batteries. *J Power Sources* **462**: 228098 (2020)

[52] Davidson J E, Hinchley S L, Harris S G, Parkin A, Parsons S, Tasker P A. Molecular dynamics simulations to aid the rational design of organic friction modifiers. *J Mol Graph Model* **25**(4): 495–506 (2006)

[53] Marichev V A. Vague concept of "reversible cleavage" in the theory of the surface tension of solids. *Surf Sci* **603**(21): 3212–3214 (2009)

**Dapeng FENG.** He received Ph.D. degree in physical chemistry in 2001 from Lanzhou Institute of Chemical Physics, Chinese Academy of Sciences (CAS), China. He is a professor at the State Key Lab of Solid Lubrication in Lanzhou Institute of Chemical Physics, CAS. He has authored or co-authored more than 80 journal papers. His research interests are high performance lubricating oil, grease, and additives. He has gained a number of awards including "Second prize of National Technical Invention" and "Technology Invention Award of Gansu Province".

**Dan QIAO.** She received her Ph.D. degree in material science in 2014 from Lanzhou Institute of Chemical Physics, CAS, China. She is an associate professor at the State Key Laboratory of Solid Lubrication in Lanzhou Institute of Chemical Physics, CAS. She has authored or co-authored more than 30 journal papers. Her research interests are ionic liquids lubricants and tribology chemistry.

**Hongxiang YU.** He received his B.S. degree in 2018 from Shandong Normal University, China. Now, he is studying for a Ph.D. degree in Lanzhou Institute of Chemical Physics, CAS, China. His current scientific interests are devoted to mechanism and kinetic analysis of tribochemical reaction of lubricants, as well as novel lubricant additives.